tvst

Article

Quantitative Assessment of Biomechanical Properties of the Human Keratoconus Cornea Using Acoustic Radiation Force Optical Coherence Elastography

Yanzhi Zhao[1,2,*], Hongwei Yang[1,2,*], Yingjie Li[1,2], Yongbo Wang[1,2], Xiao Han[3], Yirui Zhu[3], Yubao Zhang[3], and Guofu Huang[1,2]

[1] Nanchang University, Nanchang, P. R. China
[2] Department of Ophthalmology, The Third Affiliated Hospital of Nanchang University, Nanchang, P. R. China
[3] Key Laboratory of Opto-Electronic Information Science and Technology of Jiangxi Province and Jiangxi Engineering Laboratory for Optoelectronics Testing Technology, Nanchang Hangkong University, Nanchang, P. R. China

Correspondence: Yubao Zhang, Laboratory of Opto-Electronic Information Science and Technology of Nanchang Hangkong University, 696 Fenghe South Avenue, Nanchang, Jiangxi 330063, P. R. China. e-mail: zhangyubao1014@163.com
Guofu Huang, The Third Affiliated Hospital of Nanchang University, 128 Xiangshan Northern Road, Nanchang, Jiangxi 330008, P. R. China. e-mail: hgf2222@sina.com

Received: January 26, 2022
Accepted: May 10, 2022
Published: June 6, 2022

Keywords: human keratoconus cornea; biomechanical properties; optical coherence tomography; optical coherence elastography; acoustic radiation force

Citation: Zhao Y, Yang H, Li Y, Wang Y, Han X, Zhu Y, Zhang Y, Huang G. Quantitative assessment of biomechanical properties of the human keratoconus cornea using acoustic radiation force optical coherence elastography. Transl Vis Sci Technol. 2022;11(6):4, https://doi.org/10.1167/tvst.11.6.4

Purpose: Quantification of biomechanical properties of keratoconus (KC) corneas has great significance for early diagnosis and treatment of KC, but the corresponding clinical measurement remains challenging. Here, we developed an acoustic radiation force (ARF) optical coherence elastography technique and explored its potential for evaluating biomechanical properties of KC corneas.

Methods: An ARF system was used to induce the tissue deformation, which was detected by an optical coherence tomography system, and thus the localized point-by-point Young's modulus measurements were achieved. Then, two healthy rabbit eyes were imaged to test the system, after which the human keratoconus cornea was evaluated by using the same method. Three regions were selected for biomechanics analysis: the conical region, the transitional region, and the peripheral region.

Results: Young's moduli of transitional region ranged from 53.3 to 58.5 kPa. The corresponding values for the peripheral region were determined to be 58.6 kPa and 63.2 kPa, respectively. Young's moduli of the conical region were gradually increased by 18.3% from the center to the periphery, resulting in the minimum and maximum values of 44.9 kPa and 53.1 kPa, respectively. Furthermore, Young's moduli of the anterior and posterior of the center were determined to be 44.9 kPa and 50.7 kPa, respectively.

Conclusions: Differences in biomechanical properties between the three regions and slight variations within the conical region were clearly distinguished. Biomechanical weakening of the keratoconus cornea was mainly localized in the conical region, especially in the vertex position.

Translational Relevance: The system may provide a promising clinical tool for the noninvasive evaluation of local corneal biomechanics and thus may have potential applications in early keratoconus detection with further optimization.

Introduction

Biomechanical properties of the cornea, which originate from the corneal microstructure, are used to maintain its structural strength and proper geometry, so as to protect the fragile intraocular contents.[1–3] Increasing evidence shows that changes in the microstructure such as the abnormality of collagen fibrils (CFs) and proteoglycans (PGs) can result in various corneal diseases.[4–6] Therefore, a careful assessment of the corneal biomechanics can be used to study, diagnose, and treat the related disorders, such as keratoconus (KC).[7]

KC is a progressive, bilateral, asymmetric eye disease and is the most common form of corneal ectasia.[8,9] Advanced KC is mainly manifested as an apical cone-shaped protrusion of the cornea. According to the research of pathology, there is a close relationship between the corneal biomechanics and KC.[4,5,10] The results indicate that degeneration of PGs and breakage of CFs weakened biomechanical properties of the cornea, and thus the corneal structure became unstable. Moreover, corneal biomechanics have been demonstrated to be reduced in keratoconus compared to normal corneas.[11,12]

KC has annual incidence of 1:7500 with an estimated prevalence of 1:375.2.[13] It is usually developed in adolescence or early adulthood. Initially, most patients are asymptomatic, but the visual acuity progressively declines, resulting in significant vision loss due to the development of irregular astigmatism, higher-order aberration, and corneal thinning.[14] Generally, the progression of the disease can be halted by increasing corneal stiffness through corneal crosslinking (CXL).[15,16] Treatment such as CXL in the early stages of KC can minimize visual loss. Therefore, early diagnosis offers the best opportunity for effective clinical management. At present, the auxiliary methods for diagnosing keratoconus are mainly corneal topography and corneal tomography.[17] Both methods can be used to detect morphologic changes in the cornea. The Pentacam device has allowed for relatively early diagnosis by providing a range of parameters, including corneal aberrometry, elevation, thickness, and curvature.[18,19] However, studies have shown the alternation of corneal biomechanics in KC may occur before its morphologic changes.[20–23] As a result, detecting biomechanical properties may lead to a better diagnostic efficacy.[7]

Two clinically available devices for the detection of corneal biomechanics are an ocular response analyzer and corneal visualization Scheimpflug technology.[24–26] Both devices can provide the overall information by measuring the corneal deformation response following a fast air pulse, but neither can measure the local corneal biomechanics. However, according to the reference,[27–30] the hypothesis that the initiating change of KC is a focal reduction in biomechanical properties has been supported.[21] Thus, the local measurement techniques of corneal biomechanics may enable the earlier diagnosis of KC.

Elastography is a well-established method that measures local biomechanical properties of ocular tissues by detecting local tissue perturbations caused by external excitations.[31–33] The techniques based on magnetic resonance, ultrasound, and optical coherence tomography (OCT) have been widely used in biomechanics measurements.[34–36] However, both magnetic resonance and ultrasound techniques have a relatively low spatial resolution, which limits their further application. With much higher spatial resolution and sensitivity, optical coherence elastography (OCE) that employs OCT to detect local deformations is particularly suited for biomechanics imaging of ocular tissues.[37,38] Additionally, there are many excitation mechanisms, such as laser pulse,[39] air-puff,[40] and acoustic radiation force (ARF). Among them, ARF can provide noninvasive, localized, high-speed, and low-voltage excitation. Therefore, several groups have developed the ARF-OCE system for biomechanical analysis of ocular tissues,[41–44] especially the cornea.[41,44] Previous studies have shown that local biomechanical properties of healthy corneas can be precisely quantified, which suggests that ARF-OCE could be a practice method to measure biomechanical properties of the keratoconus cornea. In addition, ARF-OCE quantifies the corneal biomechanics by measuring Young's modulus, which represents the capacity of a material to resist elastic deformation, and is a classic biomechanical parameter.[20,21] Moreover, previous studies have shown that corneal Young's modulus has better predictability in detecting patients with early keratoconus.[45]

In this preliminary work, we developed an ARF-OCE system and explored its possibility of detecting the local Young's modulus of the keratoconus cornea.

Materials and Methods

System Setup

Figure 1 shows the ARF-OCE system where ARF was used to induce an elastic wave, which was captured by a swept-source OCT system. The swept-source laser used in the system has a central wavelength of 1310 nm, a sweep frequency of 50 kHz, and an average power of 19 mW. The light emitted from the laser was split into two beams through the 99:1 fiber coupler and

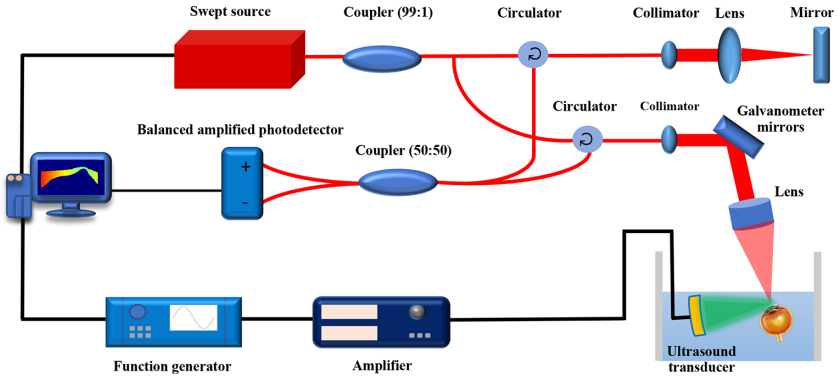

Figure 1. Schematic of the ARF-OCE system.

transmitted to the sample arm and the reference arm, respectively. In the sample arm, the circulator, collimator, dual-axis galvo system, and objective scanning lens were used to focus the light onto the sample. In the reference arm, the light was finally reflected by the reference mirror after traveling through the circulator and collimator. The backscattered and reflected lights from the two arms were gathered into the 50:50 coupler to produce interference signals that were recorded by a balanced photodetector.

The ARF excitation system includes a ring array ultrasound transducer, a function generator, and a broadband power amplifier. The working mechanism of the system can be summarized as follows. The function generator was triggered by baseline signals from the computer to create modulated sinusoidal wave signals, which were amplified by the broadband power amplifier. Finally, the amplified signals were employed to drive the ultrasonic transducer to generate ARF. The –6 dB focal spot size of the transducer was 0.78 mm (axial) and 0.70 mm (transversal).

Data Processing

The ARF-OCE system was operated in the M-B mode, wherein 500 A-lines were acquired in sequence at the same position (one M-scan). At each position, the ARF excitation was performed during the 101st and 120th A-lines. Furthermore, the ARF excitation and OCT detection were synchronized by using the λ trigger signal from the laser. After one M-scan was completed, the dual-axis galvo system was applied to move the OCT beam to the next position to perform the same M-scan. Finally, 1000 M-scans at 1000 lateral positions formed one B-scan image.

The Lamb wave model was used to quantify the biomechanical properties since the corneal thickness is small when compared with the wavelength of the generated elastic wave.[46] Equation (1) was employed to calculate the Lamb wave velocity (V_L) based on the elastic wave theory[47]:

$$V_L = \sqrt{\frac{\pi \times f \times h \times V_s}{\sqrt{3}}} \quad (1)$$

where f, h, and V_s represent the wave frequency, corneal thickness, and wave velocity, respectively.

With the relationship between Young's modulus and shear wave velocity ($E = 3 \times \rho \times V_s^2$), the Young's modulus of the cornea can be described with Equation (2):

$$E = \frac{9\rho \times V_L^4}{(\pi \times f \times h)^2} \quad (2)$$

where ρ denotes the corneal density (1087 kg/m^3 for human cornea and 1062 kg/m^3 for rabbit cornea).[48]

Sample Preparation

The Ethics Committee of the Third Affiliated Hospital of Nanchang University reviewed and approved all experiments conducted in this study.

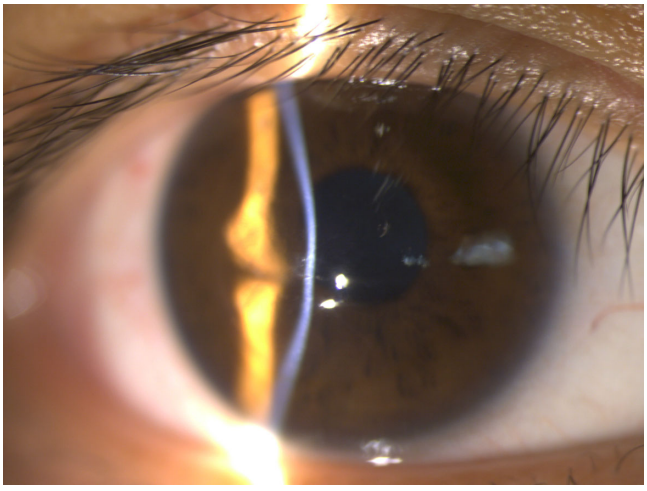

Figure 2. Slit-lamp photograph (diffuse illumination) of the eye revealed ectasia in the central cornea.

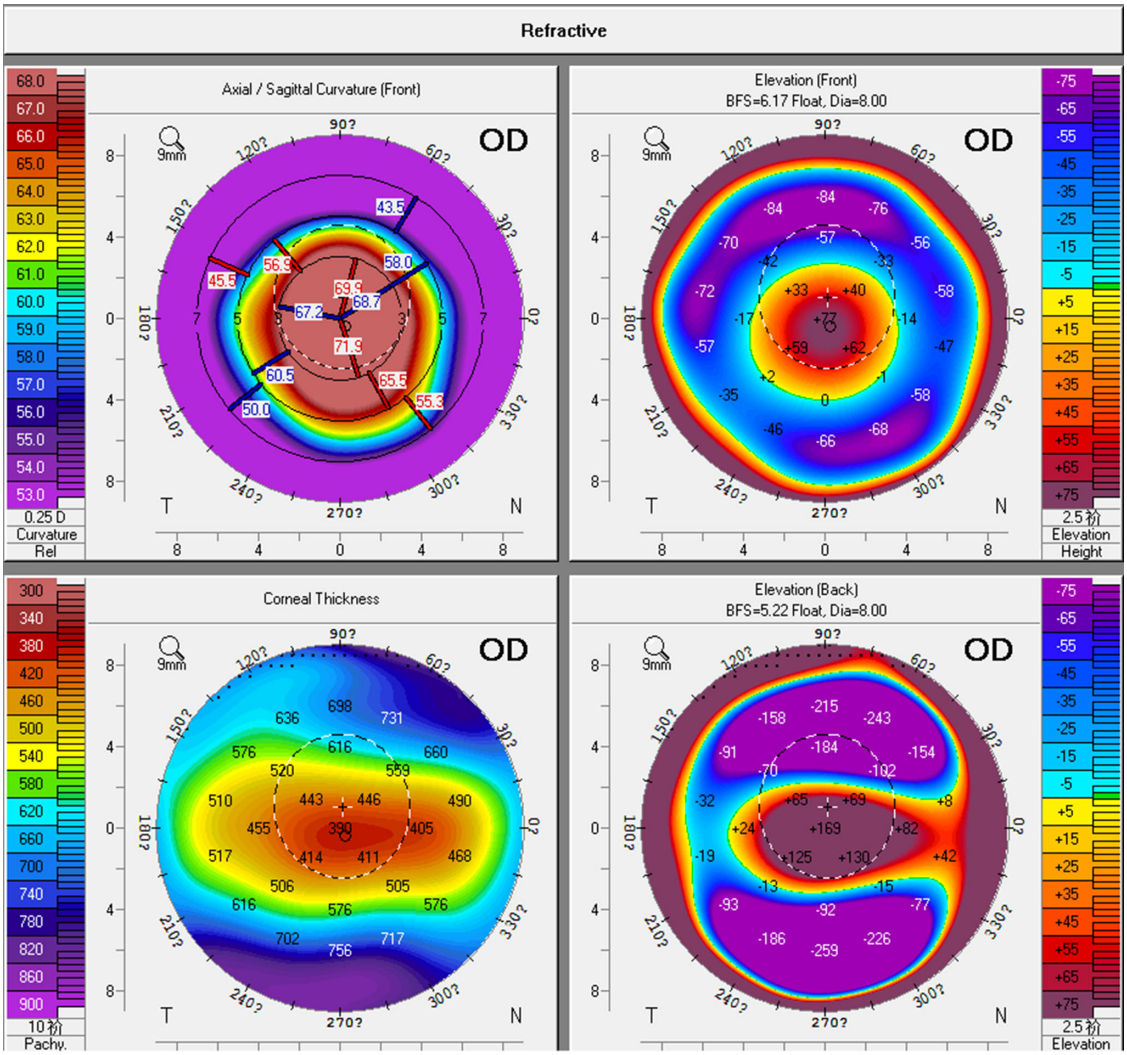

Figure 3. Corneal topography shows the characteristics of keratoconus.

Two rabbit eyes were harvested from a New Zealand white rabbit within 1 hour following euthanasia. Then, the OCE detection was carried out after removing peripheral tissues such as the ocular muscles and fat. To avoid corneal edema and hydration, experiments should be performed as soon as possible. In order to avoid eyeball shaking, the eyeball was securely fixed to an agar phantom throughout the measurement. Moreover, both the eyeball and the ultrasound transducer should be immersed in phosphate-buffered saline to preserve the normal physiologic morphology of the cornea and to provide a medium for ultrasound transmitting.

The human cornea was obtained from a KC patient who had undergone penetrating keratoplasty. Results of the preoperative examination are illustrated in Figures 2 and 3. The sample was stored at 4°C in Optisol-GS (Bausch & Lomb, NY, USA; 50006-OPT) before the OCE imaging. Then, it was mounted in the Moria artificial anterior chamber and immersed in balanced salt solution (BSS) for the same reason as the rabbit cornea. After the experiment, the KC cornea was sent to the pathology laboratory for histologic analysis.

Results

Healthy Rabbit Cornea

According to our measurements, the axial resolution, lateral resolution, imaging depth, and signal to noise ratio (SNR) were determined to be 6.71 µm, 15 µm, 4.2 mm, and 95 dB, respectively. The ARF-OCE system was first tested on healthy rabbit eyes to verify its capability to assess biomechanical properties of the cornea. The two-dimensional OCT image of the rabbit cornea was obtained, as shown in Figure 4. Subsequently, the time-lapse

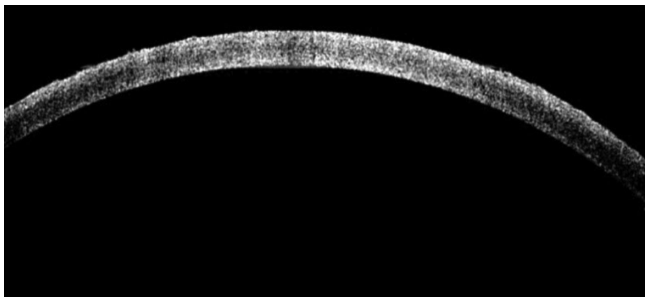

Figure 4. Two-dimensional OCT image of the healthy rabbit cornea.

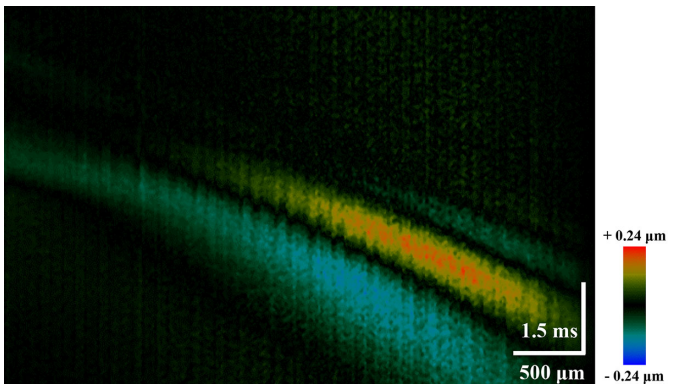

Figure 6. Spatiotemporal Doppler OCT image of the healthy rabbit cornea.

Doppler OCT images were depicted in Figure 5 to visualize the elastic wave propagation, in which different colors represent different vibration directions. The position where the elastic wave was induced can be clearly observed in Figure 5a, which is marked by a white arrow. When the elastic wave was produced, it propagated to both sides of the cornea, as indicated by the red arrows.

In order to quantify the Young's modulus, the spatiotemporal Doppler OCT image of the rabbit cornea was mapped by reslicing the Doppler OCT images. As shown in Figure 6, the horizontal axis and vertical axis represent the propagation distance and the propagation time of the elastic wave, respectively. Therefore, the elastic wave velocity was determined to be 4.03 m/s by calculating the slope of Figure 6. Then, the Young's modulus of 50.3 kPa was achieved by using Equation (2).

Human Keratoconus Cornea

After successful validations, the OCE imaging was performed on the ex vivo human cornea with KC. Figure 7 shows the two-dimensional structural image, where the cone-shaped protrusion region (conical region) can be distinguished, which is consistent with the result of histology (Fig. 8). Furthermore, to better evaluate biomechanical properties of the sample, the other two regions were also selected for analysis, including the transitional region and peripheral region. The spatiotemporal Doppler OCT images of the three regions were obtained by reslicing the time-lapse Doppler OCT images (Fig. 9), as shown in Figures 10a, 10b, and 10c, respectively. Consequently, the elastic wave velocities were determined to be 3.98 m/s, 4.23 m/s, and 4.41 m/s by calculating the slope of the spatiotemporal images, resulting in the Young's moduli of 49.1 kPa, 55.4 kPa, and 60.3 kPa, respectively. The result shows that the conical region has the softest tissue, followed by the transitional region and peripheral region in succession. With the purpose to achieve more information about the difference of corneal biomechanics, the two-dimensional distribution image of Young's modulus was depicted by directly mapping

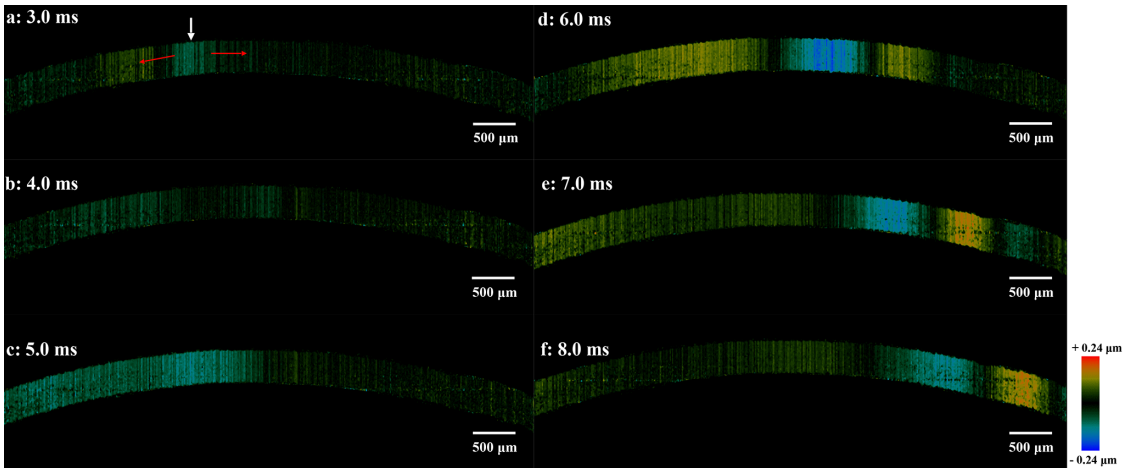

Figure 5. Time-lapse Doppler OCT B-scans of the healthy rabbit cornea.

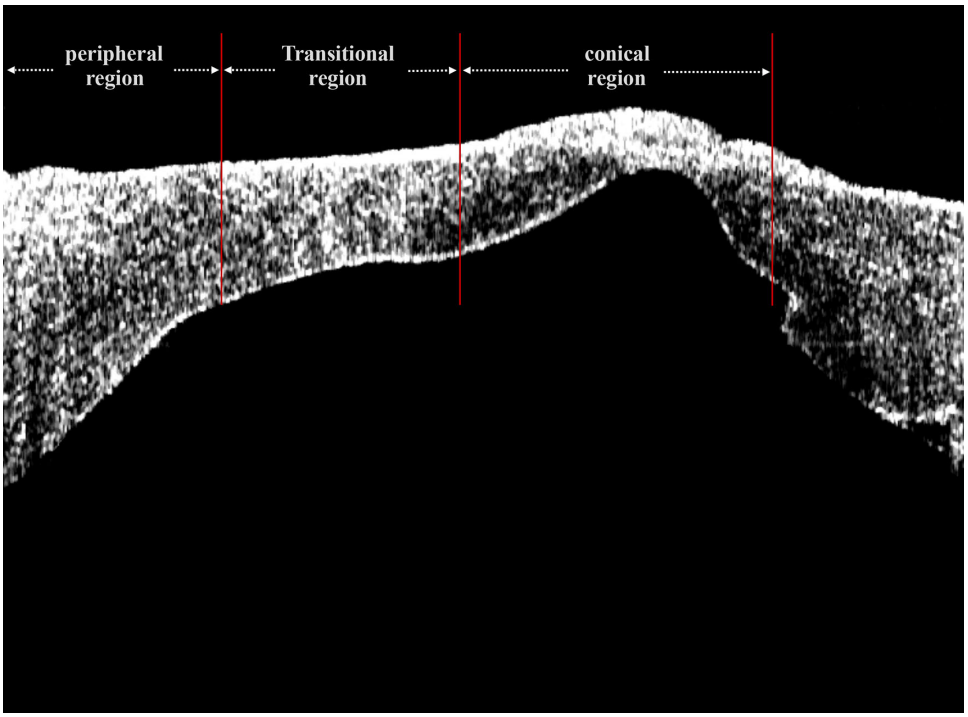

Figure 7. Two-dimensional OCT image of the human keratoconus cornea.

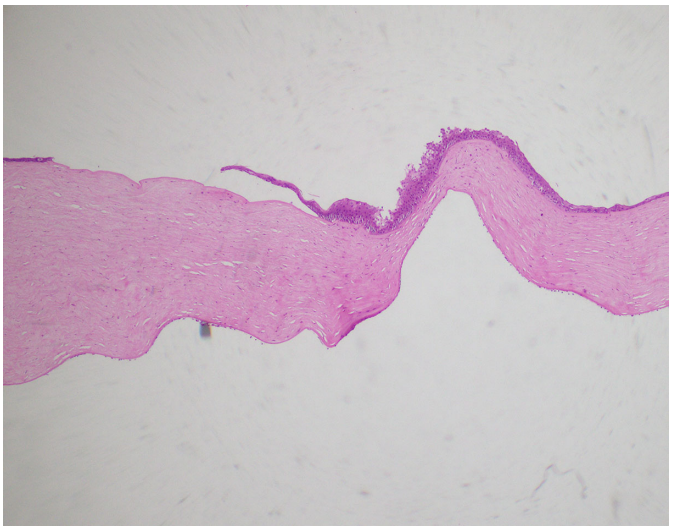

Figure 8. Hematoxylin and eosin staining at 4× magnification, with central thinning and bulging of the corneal stroma consistent with keratoconus.

the Young's modulus to the corresponding structure point to point, as shown in Figure 11. It can be found in the image that the values ranged from 44.9 to 53.1 kPa in the conical region, 53.3 to 58.5 kPa in the transitional region, and 58.6 to 63.2 kPa in the peripheral region. In addition, Young's moduli of the anterior and posterior of the center of conical region were determined to be 44.9 kPa and 50.7 kPa, respectively.

Discussion

In this preliminary study, to the best of our knowledge, we have provided the first example that uses an ARF-OCE system to quantify biomechanical properties of a human keratoconus cornea. Experiments were first conducted on healthy rabbit corneas, in which the two-dimensional OCT images and elastic wave propagations were mapped, and then the elastic wave velocity was determined. As a result, the Young's modulus was calculated to be 50.3 kPa, which is coincident with the earlier research,[49] suggesting the feasibility and reliability of our system for measuring corneal biomechanics. Based on this, a human keratoconus cornea was carefully studied by using the same method. It was found in the two-dimensional OCT image that the conical region could be observed, but it did not have a clearly defined boundary. According to the quantitative relationship between elastic wave velocity and elastic modulus, Young's moduli of the conical region, transitional region, and peripheral region (Fig. 7) were quantified. Among them, the conical region showed the smallest value, followed by the transitional region and

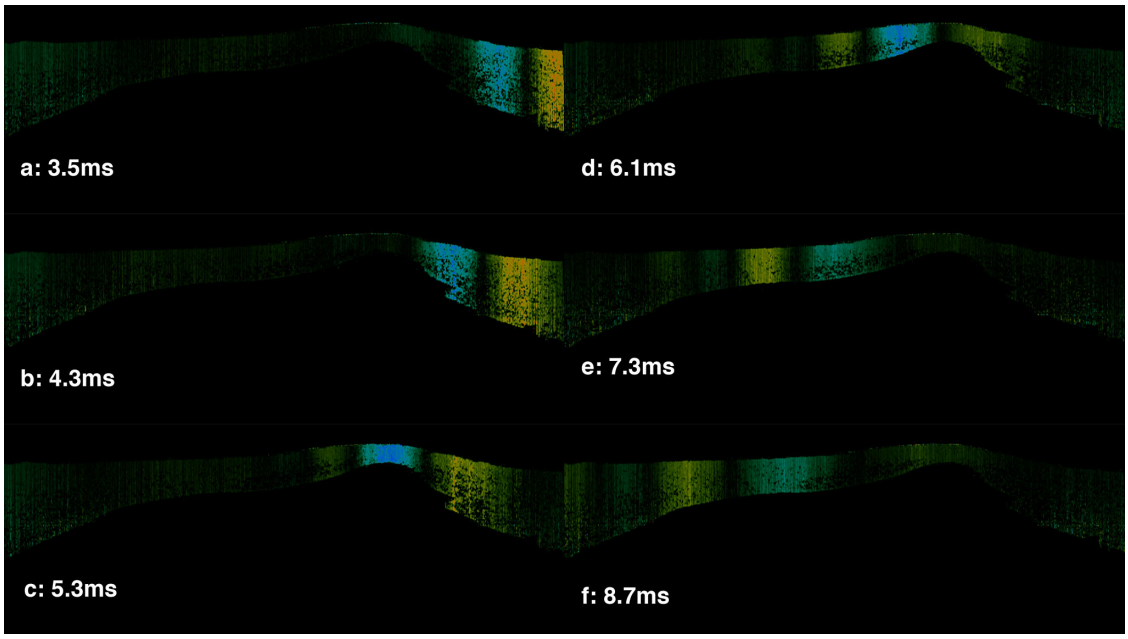

Figure 9. Time-lapse Doppler OCT B-scans of the human keratoconus cornea.

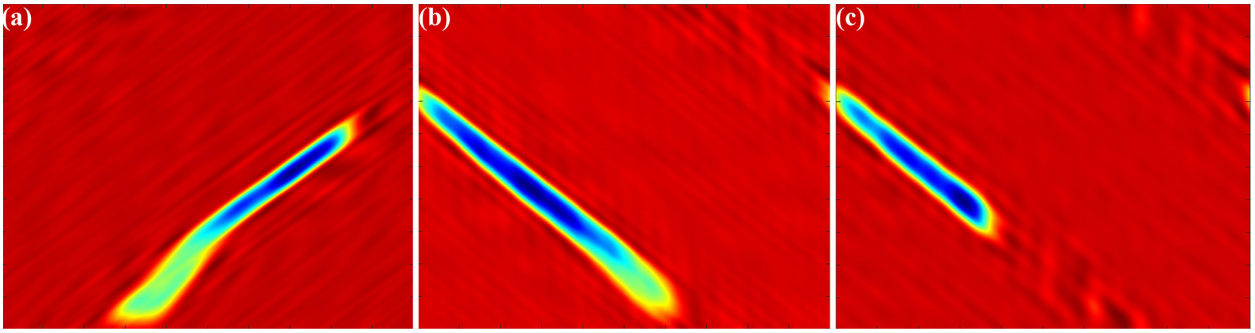

Figure 10. Spatiotemporal Doppler OCT images of the human keratoconus cornea. (a) Conical region, (b) transitional region, and (c) peripheral region.

peripheral region. Moreover, Young's modulus (60.3 kPa) of the peripheral region agreed well with that of the healthy human cornea.[50] This can be attributed to the fact that there is an obvious decrease of fiber density in the conical region.[51] In order to achieve more detailed distribution of biomechanical properties, two-dimensional Young's modulus distribution was achieved by directly mapping the elastic modulus to the corresponding structure point to point. Accordingly, the high contrast between the three regions was achieved, which made us distinguish the conical region more exactly. Furthermore, slight variations within conical region could also be identified. For example, the Young's modulus as gradually increased by 18.3% from the center to the periphery. The corresponding minimum and maximum Young's moduli were calculated to be 44.9 kPa and 53.1 kPa, respectively. It also could be found that the moduli of the anterior and posterior of the center were almost the same based on the color bar. Actually, the moduli were not exactly the same because of the color resolution limitation. The Young's moduli were determined to be 44.9 kPa and 50.7 kPa, respectively, indicating that the anterior was softer than the posterior. More biomechanics information also was revealed in the peripheral region, such as the minimum and maximum Young's moduli, which were respectively calculated to be 58.6 kPa and 63.2 kPa. It is noteworthy that the transitional region located between the conical region and peripheral region could be clearly observed, where the Young's moduli changed from 53.3 kPa to 58.5 kPa. The results indicate that our method can realize the spatial distribution of the Young's modulus of keratoconus corneas, where the detailed differences in the Young's modulus within and between the three regions could be precisely identified. This means that our system can identify

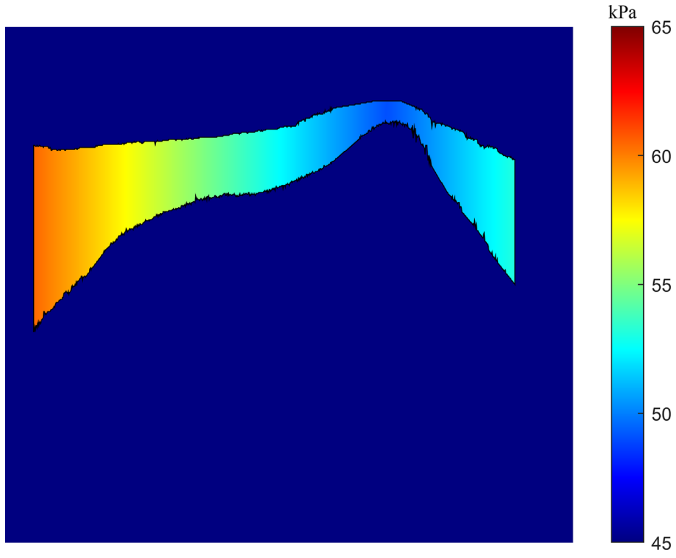

Figure 11. Two-dimensional distribution image of the Young's modulus of the human keratoconus cornea. Different colors correspond to different values of the Young's modulus, as indicated by the *color bar*.

local differences in corneal Young's modulus with high spatial resolution and sensitivity and thus has the potential to detect focal changes in corneal biomechanics of early keratoconus. With further optimization, our system may be useful to diagnose early KC, as the focal weakening in corneal biomechanics is a promising early diagnostic indicator.[30] Our work takes the first step toward this goal.

According to the related studies, certain degrees of cornea hydration were inevitable during our ex vivo experiments. However, the human keratoconus cornea was obtained immediately after penetrating keratoplasty, and thus the corneal endothelial cells were retained. Therefore, its activity could be maintained by using Optisol GS before the experiment, which is conducive to preserving the cornea in a relatively dehydrated state.[52,53] Additionally, BSS was used to preserve the normal physiologic morphology of the cornea and minimize its hydration degree. As a result, although hydration has an impact on the biomechanical properties, our results are still valuable for clinical research.

Standard CXL,[54] which effectively halts the progression of keratoconus by enhancing corneal rigidity, has been used in clinical practice for over 15 years.[15,16] However, the surgery involves extensive removal of central corneal epithelial and ultraviolet irradiation over the entire surface of the cornea, resulting in many complications such as infections and ulcerations.[55,56] This could be attributed to the fact that previous techniques were unable to quantify spatial variations in the corneal biomechanics, while the key to treating KC depends on strengthening the biomechanical properties of the conical region rather than that of the entire cornea.[21,28,57] Recently, a study used the Scheimpflug-based densitometry mark to delimit the corneal region affected in KC.[58] It would be interesting if the densitometry mark could be correlated with the spatial distribution image of the corneal biomechanics. Our study has demonstrated the potential of ARF-OCE for examinations of KC corneas. The results indicate that the biomechanical weakening is local, which mainly focuses on the small conical region, particularly the vertex position. This agrees well with the previous study.[29,51] With the features of the ARF excitation and OCT detection, our system can achieve localized point-by-point Young's modulus measurements, thus potentially allowing the precise position of the surgical area of the individual.

In this tentative study, although the efficacy of ARF-OCE for Young's modulus imaging of the human keratoconus cornea has been validated, several challenges still need to be overcome before translating the technique into clinical use. First, the current mechanical index (MI) of the ARF used in our system was about 1.0, higher than the US Food and Drug Administration ophthalmic standard for a MI of 0.23. However, the actual displacement induced by ARF in the cornea was in the submicrometer range, whereas the displacement sensitivity of our imaging system was in the subnanometer range. This indicates that it is feasible to reduce excitation force by fivefold to achieve the safety MI and remain sensitive enough to obtain a sufficient signal. Further tests will determine the minimal excitation force while maintaining adequate mechanical sensitivity. Second, the scanning speed must be increased to minimize the motion artifacts during the in vivo measurements, thus improving imaging quality. Using a swept-source laser with a faster repetition rate can provide a viable solution to this problem. Finally, the used algorithm needs to be further improved to accurately detect phase change with high sensitivity and enable a more comprehensive image reconstruction. With the optimization and development of the ARF-OCE, clinical experiments will be performed to obtain data from various stages of KC corneas and further validate the feasibility of our system for the detection of early KC.

Conclusion

In this study, we proposed the ARF-OCE system to quantify biomechanical properties of KC corneas.

The feasibility and reliability of our system were first verified with healthy rabbit eyes. Then, the measurements were performed on the human keratoconus cornea. As a result, the two-dimensional structure and Doppler OCT images, as well as the corresponding Young's moduli, were acquired. Importantly, the two-dimensional spatial distribution of Young's modulus was mapped, where detailed differences in biomechanical properties within and between the selected regions could be precisely identified. It is also found that biomechanical weakening of the cornea was mainly located in the conical region, especially in the vertex position. Our findings suggest that ARF-OCE may be a very useful method to evaluate biomechanical properties of human keratoconus corneas and could have applications in clinical medicine with further optimization.

Acknowledgments

Supported by the National Natural Science Foundation of China (12164028, 51863016), Science and Technology Infrastructure Program of Nanchang ([2019] No. 258), Traditional Chinese Medicine Research Project of Jiangxi Province (2019B072), Health and Family Planning Commission Science, and Technology Program of Jiangxi Province (20184006).

Disclosure: **Y. Zhao**, None; **H. Yang**, None; **Y. Li**, None; **Y. Wang**, None; **X. Han**, None; **Y. Zhu**, None; **Y. Zhang**, None; **G. Huang**, None

* Yanzhi Zhao and Hongwei Yang contributed equally and should be considered co-first authors.

References

1. Meek KM, Knupp C. Corneal structure and transparency. *Prog Retin Eye Res*. 2015;49:1–16.
2. Ruberti JW, Sinha Roy A, Roberts CJ. Corneal biomechanics and biomaterials. *Annu Rev Biomed Eng*. 2011;13(1):269–295.
3. Meek KM, Boote C. The use of X-ray scattering techniques to quantify the orientation and distribution of collagen in the corneal stroma. *Prog Retin Eye Res*. 2009;28(5):369–392.
4. Alkanaan A, Barsotti R, Kirat O, Khan A, Almubrad T, Akhtar S. Collagen fibrils and proteoglycans of peripheral and central stroma of the keratoconus cornea—ultrastructure and 3D transmission electron tomography. *Sci Rep*. 2019;9(1):19963.
5. Akhtar S, Bron AJ, Salvi SM, Hawksworth NR, Tuft SJ, Meek KM. Ultrastructural analysis of collagen fibrils and proteoglycans in keratoconus. *Acta Ophthalmol*. 2008;86(7):764–772.
6. Akhtar S, Alkatan HM, Kirat O, Khan AA, Almubrad T. Collagen fibrils and proteoglycans of macular dystrophy cornea: ultrastructure and 3D transmission electron tomography. *Microsc Microanal*. 2015;21(3):666–679.
7. Bao F, Geraghty B, Wang Q, Elsheikh A. Consideration of corneal biomechanics in the diagnosis and management of keratoconus: is it important? *Eye Vis*. 2016;3(1):18.
8. Rabinowitz YS. Keratoconus. *Surv Ophthalmol*. 1998;42(4):297–319.
9. Hashemi H, Heydarian S, Hooshmand E, et al. The prevalence and risk factors for keratoconus: a systematic review and meta-analysis. *Cornea*. 2020;39(2):263–270.
10. Khaled ML, Helwa I, Drewry M, Seremwe M, Estes A, Liu Y. Molecular and histopathological changes associated with keratoconus. *BioMed Res Int*. 2017;2017:1–16.
11. Andreassen T, Simonsen A, Oxlund H. Biomechanical properties of keratoconus and normal corneas. *Exp Eye Res*. 1980;31:435–441.
12. Nash I, Greene P, Foster C. Comparison of mechanical properties of keratoconus and normal corneas. *Exp Eye Res*. 1982;35:413–424.
13. Godefrooij DA, de Wit GA, Uiterwaal CS, Imhof SM, Wisse RP. Age-specific incidence and prevalence of keratoconus: a nationwide registration study. *Am J Ophthalmol*. 2017;175:169–172.
14. Gordon-Shaag A, Millodot M, Kaiserman I, et al. Risk factors for keratoconus in Israel: a case-control study. *Ophthalmic Physiol Opt*. 2015;35(6):673–681.
15. Raiskup F, Theuring A, Pillunat LE, Spoerl E. Corneal collagen crosslinking with riboflavin and ultraviolet—a light in progressive keratoconus: ten-year results. *J Cataract Refract Surg*. 2015;41(1):41–46.
16. Godefrooij DA, Gans R, Imhof SM, Wisse RPL. Nationwide reduction in the number of corneal transplantations for keratoconus following the implementation of cross-linking. *Acta Ophthalmol*. 2016;94(7):675–678.
17. Gomes JA, Tan D, Rapuano CJ, et al. Global consensus on keratoconus and ectatic diseases. *Cornea*. 2015;34(4):359–369.
18. Ruiseñor Vázquez PR, Galletti JD, Minguez N, et al. Pentacam Scheimpflug tomography findings in topographically normal patients and

subclinical keratoconus cases. *Am J Ophthalmol.* 2014;158(1):32–40.e2.
19. Castro-Luna G, Pérez-Rueda A. A predictive model for early diagnosis of keratoconus. *BMC Ophthalmol.* 2020;20(1):263.
20. Vellara HR, Patel DV. Biomechanical properties of the keratoconic cornea: a review. *Clin Exp Optom.* 2015;98(1):31–38.
21. Roberts CJ, Dupps WJ, Jr. Biomechanics of corneal ectasia and biomechanical treatments. *J Cataract Refract Surg.* 2014;40(6):991–998.
22. Ambrósio R, Jr, Lopes B, Faria-Correia F, et al. Ectasia detection by the assessment of corneal biomechanics. *Cornea*. 2016;35(7):e18–e20.
23. Sinha Roy A, Shetty R, Kummelil MK. Keratoconus: a biomechanical perspective on loss of corneal stiffness. *Indian J Ophthalmol.* 2013;61(8):392–393.
24. Fontes BM, Ambrósio R, Jr, Velarde GC, Nosé W. Ocular response analyzer measurements in keratoconus with normal central corneal thickness compared with matched normal control eyes. *J Refract Surg.* 2011;27(3):209–215.
25. Ambrósio R, Jr, Lopes BT, Faria-Correia F, et al. Integration of Scheimpflug-based corneal tomography and biomechanical assessments for enhancing ectasia detection. *J Refract Surg*. 2017;33(7):434–443.
26. Tian L, Zhang D, Guo L, et al. Comparisons of corneal biomechanical and tomographic parameters among thin normal cornea, forme fruste keratoconus, and mild keratoconus. *Eye Vis (Lond).* 2021;8(1):44.
27. Smolek MK, Klyce SD. Is keratoconus a true ectasia? An evaluation of corneal surface area. *Arch Ophthalmol*. 2000;118(9):1179–1186.
28. Pahuja N, Kumar NR, Shroff R, et al. Differential molecular expression of extracellular matrix and inflammatory genes at the corneal cone apex drives focal weakening in keratoconus. *Invest Ophthalmol Vis Sci.* 2016;57(13):5372–5382.
29. Scarcelli G, Besner S, Pineda R, Yun SH. Biomechanical characterization of keratoconus corneas ex vivo with Brillouin microscopy. *Invest Ophthalmol Vis Sci.* 2014;55(7):4490–4495.
30. Shao P, Eltony AM, Seiler TG, et al. Spatially-resolved Brillouin spectroscopy reveals biomechanical abnormalities in mild to advanced keratoconus in vivo. *Sci Rep.* 2019;9(1):7467.
31. Ophir J, Céspedes I, Ponnekanti H, Yazdi Y, Li X. Elastography: a quantitative method for imaging the elasticity of biological tissues. *Ultrason Imaging.* 1991;13(2):111–134.
32. Sarvazyan A, Hall TJ, Urban MW, Fatemi M, Aglyamov SR, Garra BS.An overview of elastography—an emerging branch of medical imaging. *Curr Med Imaging Rev.* 2011;7(4):255–282.
33. Garra BS. Elastography: history, principles, and technique comparison. *Abdom Imaging.* 2015;40(4):680–697.
34. Murphy MC, Huston J, III, Ehman RL. MR elastography of the brain and its application in neurological diseases. *Neuroimage.* 2019;187:176–183.
35. Conti CB, Cavalcoli F, Fraquelli M, Conte D, Massironi S. Ultrasound elastographic techniques in focal liver lesions. *World J Gastroenterol.* 2016;22(9):2647–2656.
36. Larin KV, Sampson DD. Optical coherence elastography—OCT at work in tissue biomechanics. *Biomed Opt Express.* 2017;8(2):1172–1202.
37. Kennedy BF, McLaughlin RA, Kennedy KM, et al. Optical coherence micro-elastography: mechanical-contrast imaging of tissue microstructure. *Biomed Opt Express.* 2014;5(7):2113–2124.
38. Kirby MA, Pelivanov I, Song S, et al. Optical coherence elastography in ophthalmology. *J Biomed Opt.* 2017;22(12):1–28.
39. Li C, Guan G, Huang Z, Johnstone M, Wang RK. Noncontact all-optical measurement of corneal elasticity. *Opt Lett.* 2012;37(10):1625–1627.
40. Li J, Wang S, Singh M, et al. Air-puff OCE for assessment of mouse cornea in vivo. *In Ophthalmic Technologies XXIV*. 2014;893004:15–19.
41. Li Y, Zhu J, Chen JJ, et al. Simultaneously imaging and quantifying in vivo mechanical properties of crystalline lens and cornea using optical coherence elastography with acoustic radiation force excitation. *APL Photonics.* 2019;4(10):106104.
42. Zhu Y, Zhang Y, Shi G, et al. Quantification of iris elasticity using acoustic radiation force optical coherence elastography. *Appl Opt.* 2020;59(34):10739–10745.
43. Qu Y, He Y, Saidi A, et al. In vivo elasticity mapping of posterior ocular layers using acoustic radiation force optical coherence elastography. *Invest Ophthalmol Vis Sci.* 2018;59(1):455–461.
44. Qu Y, Ma T, He Y, et al. Acoustic radiation force optical coherence elastography of corneal tissue. *IEEE J Sel Top Quantum Electron.* 2016;22(3):288–294.
45. Tian L, Qin X, Zhang H, et al. A potential screening index of corneal biomechanics in healthy subjects, forme fruste keratoconus patients and clinical keratoconus patients. *Front Bioeng Biotechnol*. 2021;9:766605.

46. Shih CC, Qian X, Ma T, et al. Quantitative assessment of thin-layer tissue viscoelastic properties using ultrasonic micro-elastography with Lamb wave model. *IEEE Trans Med Imaging*. 2018;37(8):1887–1898.
47. Lamb H. On waves in an elastic plate. *Proc R Soc London Ser A*. 1917;93(648):114–128.
48. Kampmeier J, Radt B, Birngruber R, Brinkmann R. Thermal and biomechanical parameters of porcine cornea. *Cornea.* 2000;19(3):355–363.
49. Han Z, Li J, Singh M, et al. Analysis of the effect of the fluid-structure interface on elastic wave velocity in cornea-like structures by OCE and FEM. *Laser Phys Lett.* 2016;13(3):035602.
50. Ramier A, Eltony AM, Chen Y, et al. In vivo measurement of shear modulus of the human cornea using optical coherence elastography. *Sci Rep*. 2020;10(1):17366.
51. Zhou D, Abass A, Lopes B, et al. Fibril density reduction in keratoconic corneas. *J R Soc Interface.* 2021;18(175):20200900.
52. Means TL, Geroski DH, Hadley A, Lynn MJ, Edelhauser HF. Viability of human corneal endothelium following Optisol-GS storage. *Arch Ophthalmol.* 1995;113(6):805–809.
53. Wagoner MD, Gonnah ES. Corneal graft survival after prolonged storage in Optisol-GS. *Cornea.* 2005;24(8):976–979.
54. Spoerl E, Huhle M, Seiler T. Induction of cross-links in corneal tissue. *Exp Eye Res*. 1998;66(1):97–103.
55. Seiler TG, Schmidinger G, Fischinger I, Koller T, Seiler T. Komplikationen der Vernetzung der Hornhaut. *Ophthalmologe*. 2013;110(7):639–644.
56. Evangelista CB, Hatch KM. Corneal collagen cross-linking complications. *Semin Ophthalmol*. 2018;33(1):29–35.
57. Hong CW, Sinha-Roy A, Schoenfield L, McMahon JT, Dupps WJ, Jr. Collagenase-mediated tissue modeling of corneal ectasia and collagen cross-linking treatments. *Invest Ophthalmol Vis Sci.* 2012;53(4):2321–2327.
58. Jiménez-García M, Ní Dhubhghaill S, Consejo A, Hershko S, Koppen C, Rozema JJ. Scheimpflug densitometry in keratoconus: a new method of visualizing the cone. *Cornea.* 2021;40(2):194–202.